TTP 97-23
June 1997

Final-State Interactions in $e^+e^- \to t\bar{t} \to bl^+\nu\bar{b}W^-$ Near Top Quark Threshold*

M. Peter and Y. Sumino†

Institut für Theoretische Teilchenphysik, Universität Karlsruhe,
D-76128 Karlsruhe, Germany

Abstract

We calculate final-state interaction corrections to the energy-angular distribution of l^+ in semi-leptonic top quark decay, where the parent top quark is produced via $e^+e^- \to t\bar{t}$ near threshold. These are the corrections due to gluon exchange between t and $\bar{b}$ ($\bar{t}$ and b) and between b and $\bar{b}$. Combining with previously known other corrections, we explicitly write down the l^+ energy-angular distribution including full $\mathcal{O}(\alpha_s) = \mathcal{O}(\beta)$ corrections near threshold. Numerical analyses of the final-state interaction corrections are presented. We find that they deform the l^+ distribution typically at 10% level. Also we elucidate mechanisms of the various effects of the final-state interactions. We find that all qualitative features of the numerical results can be understood from intuitive pictures. The natures that $\bar{b}$ is emitted preferrably in the parent $\bar{t}$'s spin direction and that there is attractive force between $\bar{b}$ and $\bar{t}$ generate: shift of $|\mathbf{p}_t|$-distribution, forward-backward asymmetry of t, modification of the top-quark polarization vector, and energy-angle-correlated deformation of l^+ distributions.

*Contributed paper to XVIII International Symposium on Lepton-Photon Interactions, Hamburg, Germany, 28 July - 1 August 1997.

†On leave of absence from Department of Physics, Tohoku University, Sendai 980-77, Japan.

1 Introduction

The study of the top quark at a future e^+e^- linear collider in the $t\bar{t}$ threshold region will be one of the unique testing grounds for unraveling the properties of the top quark. So far there have been a number of studies of the cross sections in the $t\bar{t}$ threshold region, both theoretical and experimental [1]-[18]. It has been recognized that the threshold region is rich in physics and also is apt for extracting various physical parameters efficiently (m_t, α_s, Γ_t, m_H, g_{tH}, etc.).

While most of the previous analyses were concerned with the production process of the top quark, one may also analyze the decay process in detail and extract some important physics information. Especially the fact that t and $\bar{t}$ are produced highly polarized in the threshold region is potentially quite advantageous for studying the electroweak properties of the top quark through its decay processes. Detailed studies of the decay of free polarized top quarks have already been available including the full $\mathcal{O}(\alpha_s)$ corrections [15, 20]. In the threshold region, however, these precise analyses do not apply directly because of the existence of corrections unique to this region, which connect the production and decay processes of the top quark. Namely, these are the corrections due to gluon exchange between t and $\bar{b}$ ($\bar{t}$ and b) or between b and $\bar{b}$.

This type of corrections arises when the produced particles decay quickly into many particles, and are referred to as "final-state interactions", or "rescattering corrections", or "non-factorizable corrections" in the literature. They generally vanish in inclusive cross sections [9, 10, 11], but modify the shape of differential distributions in a non-trivial manner [10, 14, 18]. The size of the corrections is at the 10% level in the $t\bar{t}$ threshold region, so that it is inevitable to incorporate their effects in the precision studies of top-quark decays near threshold. The same kind of effects have recently been studied in W pair-production [25, 26].

The first study of the top-quark decay in the threshold region was given as a part of the results in Ref. [18], where the mean value $\langle n\ell \rangle$ of the charged lepton l^+ four-momentum projection on an arbitrarily chosen four-vector n in semi-leptonic top decays is proposed as an experimentally observable quantity sensitive to top quark polarization and is calculated including the final-state interactions. Clearly, and also admittedly in that paper, the calculation of the differential distribution of l^+ including the final-state interactions has been demanded.

In this paper, we calculate the final-state interaction corrections to the differential energy-angular distribution of l^+ in semi-leptonic top quark decays in the $t\bar{t}$ threshold region. We find that these corrections deform the l^+ distribution non-trivially at the 10% level. Combining with other previously known results, we write down explicitly the formula for the energy-angular distribution of l^+ including all $\mathcal{O}(\alpha_s) = \mathcal{O}(\beta)$ corrections near $t\bar{t}$ threshold.

Another main achievement of this paper is the presentation of physical descriptions of the final-state interactions which enable us to understand the qualitative features of our numerical results. It turns out that one may explain various effects of the final-state interactions on the differential distributions by following the classical picture that there is an attractive force between t and $\bar{b}$ (or between $\bar{t}$ and b). Such descriptions would be useful since the systematic calculation of the final-state interactions based on quantum field theory is rather complicated, involving box and pentagon-type diagrams, and it is not easy to make physical sense directly out of the obtained final expression. To our knowledge these qualitative explanations have never been put forth although corresponding theoretical calculations and numerical studies have been available partly.

In section 2 we introduce some notations necessary for later sections. Section 3 gives physical descriptions of the effects of final-state interactions. The results of the systematic calculations of final-state interaction corrections to the l^+ energy-angular distribution, as well as the complete formula for the distribution including all $\mathcal{O}(\alpha_s) = \mathcal{O}(\beta)$ corrections, are given in section 4. A detailed account of our calculational methods will be published elsewhere. Section 5 shows various numerical results and a comparison with the qualitative picture. Conclusion and discussion are presented in section 6.

2 Preparations

In this section we introduce some notations to be used in this paper.

We consider longitudinally polarized e^+e^- beams throughout our analyses. $P_{e^\pm}$ denotes the longitudinal polarization of $e^\pm$, and we set

$$\chi = \frac{P_{e^+} - P_{e^-}}{1 - P_{e^+} P_{e^-}}. \tag{2.1}$$

We choose a reference coordinate system in the $t\bar{t}$ c.m. frame. Three orthonormal basis vectors are defined as

$$\begin{aligned} \hat{\mathbf{n}}_{\parallel} &= \frac{\mathbf{p}_{e^-}}{|\mathbf{p}_{e^-}|} \\ \hat{\mathbf{n}}_{\mathrm{N}} &= \frac{\mathbf{p}_{e^-} \times \mathbf{p}_t}{|\mathbf{p}_{e^-} \times \mathbf{p}_t|} \\ \hat{\mathbf{n}}_{\perp} &= \hat{\mathbf{n}}_{\mathrm{N}} \times \hat{\mathbf{n}}_{\parallel}\ , \end{aligned} \tag{2.2}$$

where $\mathbf{p}_{e^-}$ and $\mathbf{p}_t$ represent the e^- and t momentum, respectively.

Our conventions for the fermion vector and axial-vector couplings to the Z boson are

$$v_f = 2I_f^3 - 4q_f \sin^2\theta_{\mathrm{W}}, \qquad a_f = 2I_f^3, \tag{2.3}$$

respectively. Certain combinations of these couplings will be useful below:

$$\begin{aligned} a_1 &= q_e^2 q_t^2 + (v_e^2 + a_e^2) v_t^2 d^2 + 2 q_e q_t v_e v_t d \\ a_2 &= 2 v_e a_e v_t^2 d^2 + 2 q_e q_t a_e v_t d \\ a_3 &= 4 v_e a_e v_t a_t d^2 + 2 q_e q_t a_e a_t d \\ a_4 &= 2(v_e^2 + a_e^2) v_t a_t d^2 + 2 q_e q_t v_e a_t d, \\ d &= \frac{1}{16 \sin^2\theta_{\mathrm{W}} \cos^2\theta_{\mathrm{W}}} \frac{s}{s - M_Z^2}, \end{aligned} \tag{2.4}$$

and

$$\begin{aligned} C_{\parallel}^0(\chi) &= -\frac{a_2 + \chi a_1}{a_1 + \chi a_2}, & C_{\parallel}^1(\chi) &= \left(1 - \chi^2\right) \frac{a_2 a_3 - a_1 a_4}{(a_1 + \chi a_2)^2}, \\ C_{\perp}(\chi) &= -\frac{1}{2} \frac{a_4 + \chi a_3}{a_1 + \chi a_2}, & C_{\mathrm{N}}(\chi) &= -\frac{1}{2} \frac{a_3 + \chi a_4}{a_1 + \chi a_2} \ = \ -C_{\mathrm{FB}}(\chi). \end{aligned} \tag{2.5}$$

Finally, we define

$$y = \frac{M_W^2}{m_t^2}, \qquad \kappa = \frac{1-2y}{1+2y}. \tag{2.6}$$

The QCD enhancement of the top-quark production cross section near threshold is incorporated through the S-wave and P-wave Green's functions, $\tilde{G}(p,E)$ and $\tilde{F}(p,E)$, of the non-relativistic Schrödinger equations in the presence of the QCD potential. These functions are defined by

$$\left[-\frac{\nabla^2}{m_t} + V_{QCD}(r) - (E+i\Gamma_t)\right] G(\mathbf{x},E) = \delta^3(\mathbf{x}), \tag{2.7}$$

$$\left[-\frac{\nabla^2}{m_t} + V_{QCD}(r) - (E+i\Gamma_t)\right] F^k(\mathbf{x},E) = -i\partial^k\delta^3(\mathbf{x}), \tag{2.8}$$

and

$$\tilde{G}(p,E) = \int d^3\mathbf{x}\, e^{-i\mathbf{p}\cdot\mathbf{x}}\, G(\mathbf{x},E), \tag{2.9}$$

$$p^k\,\tilde{F}(p,E) = \int d^3\mathbf{x}\, e^{-i\mathbf{p}\cdot\mathbf{x}}\, F^k(\mathbf{x},E). \tag{2.10}$$

One may obtain the Green's functions either by first solving the Schrödinger equations in coordinate space and taking the Fourier transforms of the solutions [3], or by solving the Schrödinger equations directly in momentum space [5].

Various known $\mathcal{O}(\alpha_s)$ corrections to threshold cross sections can also be expressed in terms of the above Green's functions. In Ref. [18] the following functions have been defined, which are solely determined from QCD, to represent various independent corrections. We will pursue the same conventions in this paper.

$$\varphi(p,E) = \frac{(1-C_F\alpha_s/\pi)}{(1-2C_F\alpha_s/\pi)}\,\frac{p}{m_t}\,\frac{\tilde{F}^*(p,E)}{\tilde{G}^*(p,E)}, \tag{2.11}$$

$$\varphi_{\rm R} = {\rm Re}\,\varphi, \qquad \varphi_{\rm I} = {\rm Im}\,\varphi, \tag{2.12}$$

$$\psi_1(p,E) = -\,C_F\cdot 4\pi\alpha_s \int \frac{d^3\mathbf{q}}{(2\pi)^3}\,\frac{1}{|\mathbf{q}-\mathbf{p}_t|^3}\,2\,{\rm Im}\left[\frac{\tilde{G}(q,E)}{\tilde{G}(p,E)}\right]\cdot\frac{\pi}{2} \tag{2.13}$$

$$\psi_{\rm R}(p,E) = -\,C_F\cdot 4\pi\alpha_s\,{\rm Pr.}\int \frac{d^3\mathbf{q}}{(2\pi)^3}\,\frac{1}{|\mathbf{q}-\mathbf{p}_t|^3}\,\frac{\mathbf{p}_t\cdot(\mathbf{q}-\mathbf{p}_t)}{|\mathbf{p}_t|\,|\mathbf{q}-\mathbf{p}_t|}\,2\,{\rm Re}\left[\frac{\tilde{G}(q,E)}{\tilde{G}(p,E)}\right]. \tag{2.14}$$

Here $C_F = 4/3$ is a color factor; $p = |\mathbf{p}_t|$ and $q = |\mathbf{q}|$. Eqs. (2.13) and (2.14)* differ slightly in their integrands from those defined in Ref. [18]. The differences, however, can be regarded as higher order corrections which are beyond the scope of our analysis.

*One may render Eqs. (2.13) and (2.14) to one-parameter integral forms by integrating over $d\Omega_{\mathbf{q}}$ explicitly [10].

3 Qualitative Description of Final-State Interaction Effects

In this section a qualitative understanding of the effects of final-state interactions is explained. It is based on the classical picture that t and $\bar{b}$ ($\bar{t}$ and b) attract each other due to the interaction. We will see that all the following qualitative features match well with our numerical studies presented in section 5.

3.a Top Momentum Distribution

First let us consider the effect of final-state interactions on the top-quark momentum ($|\mathbf{p}_t|$) distribution, where $\mathbf{p}_t$ is reconstructed from the bW^+ momenta at time $\tau \to \infty$. The energy of a $t\bar{t}$ system before its decay is given by

$$\mathcal{E} = E_t + E_{\bar{t}} + V(|\mathbf{r}_t - \mathbf{r}_{\bar{t}}|), \tag{3.1}$$

where

$$E_t = m_t + \frac{\mathbf{p}_t^2}{2m_t}, \qquad E_{\bar{t}} = m_t + \frac{\mathbf{p}_{\bar{t}}^2}{2m_t}, \qquad V(r) = -C_F\frac{\alpha_s}{r}. \tag{3.2}$$

Suppose t decays first and let $a \sim (\alpha_s m_t)^{-1} \sim (m_t\Gamma_t)^{-1/2}$ be the typical distance between t and $\bar{t}$ at the time of t decay. Then, just before the decay, the momenta of t and $\bar{t}$ are given by

$$|\mathbf{p}_t| = |\mathbf{p}_{\bar{t}}| \sim \sqrt{m_t\,[\mathcal{E} - 2m_t + |V(a)|\,]}. \tag{3.3}$$

Their order of magnitude is $\alpha_s m_t \sim$ (Bohr radius)$^{-1}$. If it were not for the final-state interactions between $\bar{t}$ and b, and if $\bar{t}$, b and W^+ travelled as free particles, the above momentum would be transferred to the bW^+ system at time $\tau \to \infty$:

$$|\mathbf{p}_b + \mathbf{p}_{W^+}|_{\tau\to\infty} \sim \sqrt{m_t\,[\mathcal{E} - 2m_t + |V(a)|\,]}. \tag{3.4}$$

Taking into account the final-state interaction (Coulomb interaction) between $\bar{t}$ and b, the energy of $\bar{t}bW^+$ system is given by*

$$\mathcal{E} = E_b + E_{W^+} + E_{\bar{t}} + V(|\mathbf{r}_b - \mathbf{r}_{\bar{t}}|), \tag{3.5}$$

$$E_b = |\mathbf{p}_b|, \qquad E_{W^+} = \sqrt{\mathbf{p}_{W^+}^2 + M_W^2}. \tag{3.6}$$

As depicted in Fig. 1, the tracks of b and $\bar{t}$ are deflected due to the attraction between the two particles, which lose kinetic energy as b flies off to infinity at the speed of light. The classical equation of motion is given by

$$\frac{d\mathbf{p}_b}{d\tau} = -\frac{d\mathbf{p}_{\bar{t}}}{d\tau} = -\frac{\partial}{\partial\mathbf{r}_b}V(|\mathbf{r}_b - \mathbf{r}_{\bar{t}}|). \tag{3.7}$$

*Here we neglect the interaction of $\bar{t}$ (b) and magnetic field generated by b ($\bar{t}$). This approximation is justified in the case of our interest; see section 4.

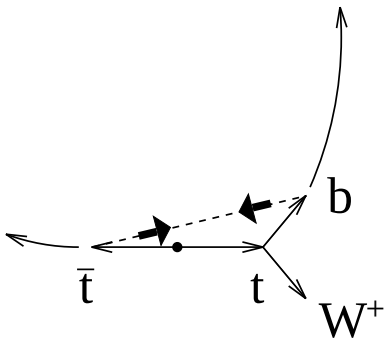

Figure 1: Attractive Coulomb force between $\bar{t}$ and b (from t decay). The momentum transfer $\delta\mathbf{p}_b = -\delta\mathbf{p}_{\bar{t}}$ due to the attraction is indicated by thick arrows.

Substituting the free particle solution $\mathbf{r}_b = \mathbf{v}\tau + \mathbf{r}_0$ on the right-hand side and noting $|\mathbf{r}_b - \mathbf{r}_{\bar{t}}| \simeq \tau$, we may estimate the size of the momentum transfer due to the attractive force as[†]

$$|\delta\mathbf{p}_b| = |\delta\mathbf{p}_{\bar{t}}| \sim |V(r_{min})|, \tag{3.8}$$

where the minimum distance between b and $\bar{t}$ is denoted as r_{min}. Typically $r_{min} \sim a$, and we find from Eq. (3.8) that the effect of final-state interactions on the $|\mathbf{p}_t|$ distribution is of the order of $|\delta\mathbf{p}_t| \sim \alpha_s^2 m_t$. Obviously the effect is to reduce $|\mathbf{p}_t|$.

3.b Forward-Backward Asymmetric Distribution

Next we consider the $\cos\theta_{te}$ distribution of the top quark. (θ_{te} denotes the angle between t and e^- in the $t\bar{t}$ c.m. frame.) It has been known that a forward-backward asymmetric distribution of the top quark is generated by the final-state interactions [10, 18]. We describe its mechanism here.

We consider the case where $\bar{t}$ decays first and examine the interaction between t and $\bar{b}$. Approximately, the t and $\bar{t}$ pair-produced near threshold in e^+e^- collisions have their spins parallel or anti-parallel to the e^- beam direction and the spins of t and $\bar{t}$ are always oriented parallel to each other. In fact in leading order the polarization vector of the top quark is given by[16] $\boldsymbol{\mathcal{P}} = C_{||}^0(\chi)\,\hat{\mathbf{n}}_{||}$. On the other hand, the decay of $\bar{t}$ occurs via a $V-A$ coupling, and $\bar{b}$ is emitted preferably in the spin direction of the parent $\bar{t}$, see Fig. 2. More precisely, the excess of the $\bar{b}$'s emitted in the $\bar{t}$ spin direction over those emitted in the opposite direction is given by κ defined in Eq. (2.6). Suppose t and $\bar{t}$ have their spins in the $\hat{\mathbf{n}}_{||}$ direction. Then $\bar{b}$ will be emitted dominantly in the $\hat{\mathbf{n}}_{||}$ direction. One can see from Fig. 3(a) that in this case t is always attracted to the forward direction ($\bar{b}$ is attracted to the backward direction) due to the attractive force between t and $\bar{b}$. The direction of the attractive force will be opposite if t and $\bar{t}$ have their spins in the $-\hat{\mathbf{n}}_{||}$ direction. Thus, polarized top quarks will be pulled in a definite (forward or backward) direction, and we may expect that a forward-backward asymmetric distribution of the top quark $\sim \kappa\, C_{||}^0(\chi)\cos\theta_{te}$ is generated by the final-state interaction.

[†] It corresponds to solving the equation of motion by a series expansion of α_s.

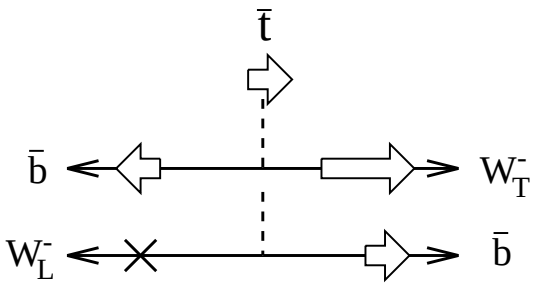

Figure 2: Typical configurations in the decay of $\bar{t}$ with definite spin orientation. Transverse W^- (W_T^-) tend to be emitted in the direction of the $\bar{t}$ spin orientation, while longitudinal W^- (W_L^-) are emitted in the opposite direction due to helicity conservation. For $m_t \simeq 175$ GeV, $\bar{t}$ decays mainly to W_L^-, hence $\bar{b}$ is emitted more in the $\bar{t}$ spin direction.

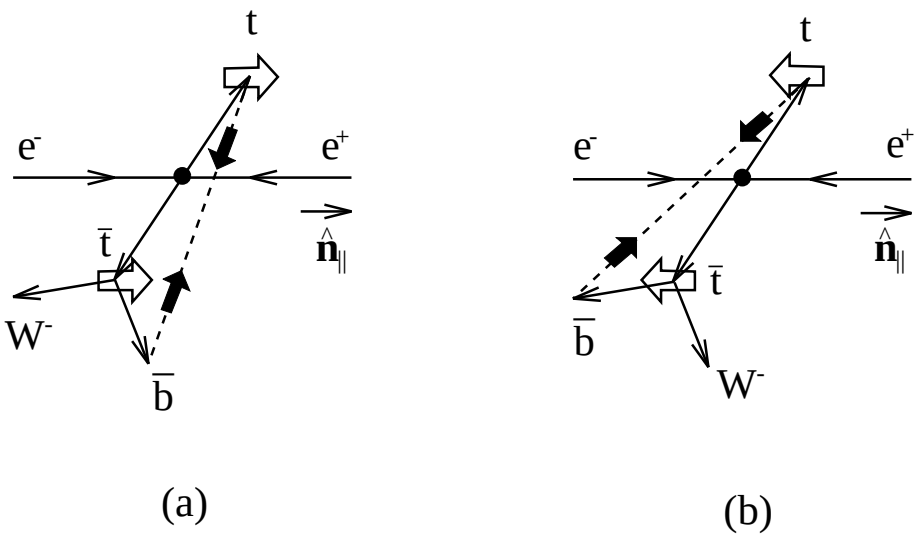

Figure 3: Attractive force between t and $\bar{b}$ when the t and $\bar{t}$ spins are oriented in the (a)$\hat{\mathbf{n}}_{||}$ direction, and in the (b)$-\hat{\mathbf{n}}_{||}$ direction. The momentum transfer $\delta\mathbf{p}_b = -\delta\mathbf{p}_{\bar{t}}$ due to the attraction is indicated by thick black arrows.

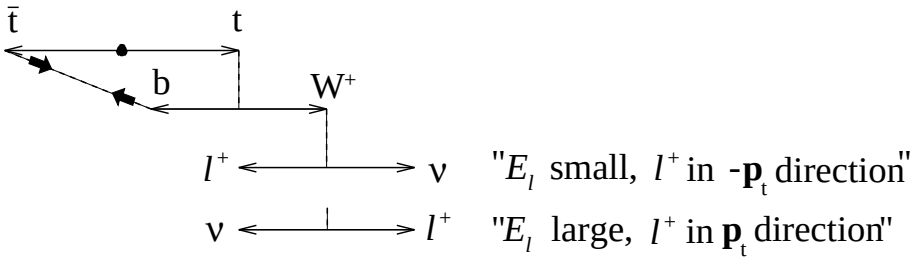

Figure 4: Typical configurations of the particles in semi-leptonic decay of t when the b-quark is emitted in the $\bar{t}$ direction. Due to the boost by W^+, the energy-angle correlation of l^+ will be either "E_l is small and l^+ emitted in $-\mathbf{p}_t$ direction" or "E_l is large and l^+ emitted in $\mathbf{p}_t$ direction".

Incidentally, a forward-backward asymmetric distribution of the top quarks is also generated by the interference between the S-wave and P-wave $t\bar{t}$ pair-production amplitudes [4]. It is formally a quantity of the same order as the final-state interaction near threshold, since it arises as an $\mathcal{O}(\alpha_s) = \mathcal{O}(\beta)$ correction to the leading spherically symmetric distribution. Interestingly, we find that each $\cos\theta_{te}$ distribution has quite a different physical explanation for its generation mechanism, although it is a common feature that both originate from the interplay between QCD and electroweak interactions.

3.c Top Quark Polarization Vector

The Coulomb attraction between t and $\bar{b}$ also modifies the top-quark polarization vector [18]. As we have seen previously, in the $\bar{t}$ decay, $\bar{b}$ tends to be emitted in the direction of the parent $\bar{t}$'s spin direction (Fig. 2). We then find from Fig. 3 that if the t and $\bar{t}$ spins are oriented in the $\hat{\mathbf{n}}_{||}$ direction, t will be attracted to the forward direction due to the attraction by $\bar{b}$, and oppositely attracted to the backward direction if the t and $\bar{t}$ spins are in the $-\hat{\mathbf{n}}_{||}$ direction. This means that in the forward region ($\cos\theta_{te} \simeq 1$) the number of t's with spin in $\hat{\mathbf{n}}_{||}$ direction increases whereas in the backward region the number of those with spin in the opposite direction increases. Or equivalently, the $\hat{\mathbf{n}}_{||}$-component of the top-quark polarization vector increases in the forward region and decreases in the backward region. We may thus conjecture that the top-quark polarization vector is modified as $\delta\mathcal{P} \sim \kappa \cos\theta_{te}\, \hat{\mathbf{n}}_{||}$ due to the interaction between t and $\bar{b}$.

3.d l^+ Energy-Angular Distribution

Finally let us examine the effect of the Coulomb attraction between b and $\bar{t}$ on the l^+ energy-angular distribution in the semi-leptonic decay of t. The b-quark from t decay will be attracted in the direction of $\bar{t}$ due to the Coulomb interaction between these two particles. We show schematically typical configurations of the particles in the top-quark semi-leptonic decay in Fig. 4. It can be seen that if the probability for b being emitted in the $\bar{t}$ direction increases, correspondingly the probability for particular l^+ energy-angular configurations increases. These

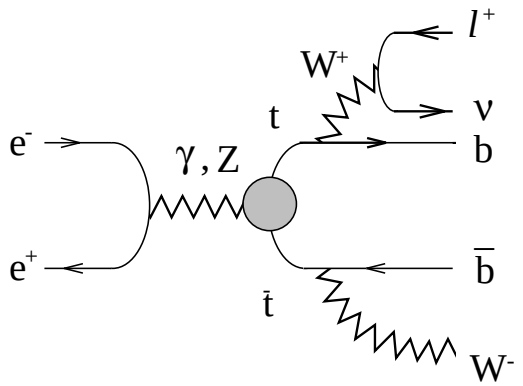

Figure 5: Born-type diagram for the process $e^+e^- \to t\bar{t} \to bl^+\nu\bar{b}W^-$.

configurations are either "E_l is small and l^+ emitted in $-\mathbf{p}_t$ direction" or "E_l is large and l^+ emitted in $\mathbf{p}_t$ direction".

4 l^+ Energy-Angular Distribution

We present the formulas for the charged lepton energy-angular distribution in the decay of a top quark that is produced via $e^+e^- \to t\bar{t}$ near threshold. In the following, $x_l = 2E_l/m_t$ and Ω_l, respectively, denote the normalized energy and solid angle of the charged lepton as defined in the rest frame of the parent top quark. For simplicity we neglect the decay of W^- in our calculations.

4.a Factorizable Part

It is well-known that the contribution of the Born-type (reducible) diagram (Fig. 5) to the differential distribution of t and l^+ has a form where the production and decay processes of the top quark are factorized:

$$\frac{d\sigma_{\rm Born}(e^+e^- \to t\bar{t} \to bl^+\nu\bar{b}W^-)}{d^3\mathbf{p}_t dx_l d\Omega_l} = \frac{d\sigma_{\rm Born}(e^+e^- \to t\bar{t})}{d^3\mathbf{p}_t} \times \frac{1}{\Gamma_t} \frac{d\Gamma_{t\to bl^+\nu}(\boldsymbol{\mathcal{P}}_{\rm Born})}{dx_l d\Omega_l}. \tag{4.1}$$

The above factorized form holds true even including $\mathcal{O}(\alpha_s) = \mathcal{O}(\beta)$ corrections to each vertex and propagator in the Born-type diagram. Here, Γ_t[21, 24] and $d\Gamma_{t\to bl^+\nu}(\boldsymbol{\mathcal{P}}_{\rm Born})/dx_l d\Omega_l$[23, 15], respectively, are the width of a free top quark and the charged lepton (l^+) energy-angular distribution in the decay of a free polarized top quark, both including full $\mathcal{O}(\alpha_s)$ corrections. Near threshold, the top-quark production cross section for longitudinally polarized e^+e^- beams is given by[18]

$$\frac{d\sigma_{\rm Born}(e^+e^- \to t\bar{t})}{d^3\mathbf{p}_t} = \frac{d\sigma^0_{t\bar{t}}}{d^3\mathbf{p}_t} \times \left[1 + 2C_{FB}(\chi)\varphi_{\rm R}(p,E)\cos\theta_{te}\right], \tag{4.2}$$

$$\frac{d\sigma^0_{t\bar{t}}}{d^3\mathbf{p}_t} = \frac{N_c\alpha^2\Gamma_t}{4\pi m_t^4}\,(1-P_{e^+}P_{e^-})\,(a_1+\chi a_2)\left(1-\frac{4C_F\alpha_s}{\pi}\right)\left|\tilde{G}(p,E)\right|^2. \tag{4.3}$$

Here, α is the fine structure constant, and $N_c = 3$. $\boldsymbol{\mathcal{P}}_{\rm Born} = \mathcal{P}_{||}\hat{\mathbf{n}}_{||} + \mathcal{P}_{\perp}\hat{\mathbf{n}}_{\perp} + \mathcal{P}_{\rm N}\hat{\mathbf{n}}_{\rm N}$ represents the polarization vector of a top quark produced via the Born-type diagram (Fig. 5) near threshold. The components are given by

$$\mathcal{P}_{||}(\mathbf{p}_t,E,\chi) = C^0_{||}(\chi) + C^1_{||}(\chi)\,\varphi_{\rm R}(p,E)\,\cos\theta_{te} \tag{4.4}$$
$$\mathcal{P}_{\perp}(\mathbf{p}_t,E,\chi) = C_{\perp}(\chi)\,\varphi_{\rm R}(p,E)\,\sin\theta_{te} \tag{4.5}$$
$$\mathcal{P}_{\rm N}(\mathbf{p}_t,E,\chi) = C_{\rm N}(\chi)\varphi_{\rm I}(p,E)\sin\theta_{te}\,. \tag{4.6}$$

4.b Final-state Interaction Corrections

Corrections due to the final-state interactions (rescattering corrections) that originate from the irreducible diagrams (a)-(d) in Fig. 6 are important particularly in the threshold region. In fact their contributions are counted as $\mathcal{O}(\alpha_s) = \mathcal{O}(\beta)$ corrections to the leading threshold enhancement[10]. We list the effect of each diagram on the l^+ energy-angular distribution. We chose Coulomb-gauge for the QCD part in our calculations.

The contribution of diagram (a) (exchange of one Coulomb-gluon between t and $\bar{b}$) can be regarded, after integrating over $\bar{b}W^-$ phase-space, as a correction to the production process of t. Thus, the production cross section $d\sigma_{\rm Born}(e^+e^-\to t\bar{t})/d^3\mathbf{p}_t$ and the polarization vector $\boldsymbol{\mathcal{P}}_{\rm Born}$ of the top quark receive corrections by this diagram, whereas the decay distribution $d\Gamma_{t\to bl^+\nu}(\boldsymbol{\mathcal{P}}_{\rm Born})/dx_l d\Omega_l$ remains unaffected (except for the modification of $\boldsymbol{\mathcal{P}}_{\rm Born}$). In fact the contribution of this diagram can be incorporated by the following substitutions in Eq. (4.1):

$$\frac{d\sigma_{\rm Born}(e^+e^-\to t\bar{t})}{d^3\mathbf{p}_t} \to \frac{d\sigma_{\rm Born}(e^+e^-\to t\bar{t})}{d^3\mathbf{p}_t}\times(1+\delta_a)\,, \qquad \boldsymbol{\mathcal{P}}_{\rm Born}\to\boldsymbol{\mathcal{P}}_{\rm Born}+\delta\boldsymbol{\mathcal{P}}_a \tag{4.7}$$

with

$$\delta_a = \frac{1}{2}\left[\psi_1(p,E) + \kappa C^0_{||}\psi_{\rm R}(p,E)\cos\theta_{te}\right], \tag{4.8}$$
$$\delta\boldsymbol{\mathcal{P}}_a = \frac{1}{2}\left[1-(C^0_{||})^2\right]\kappa\,\psi_{\rm R}(p,E)\cos\theta_{te}\cdot\hat{\mathbf{n}}_{||}. \tag{4.9}$$

Diagram (b) (exchange of one Coulomb-gluon between $\bar{t}$ and b) in Fig. 6 gives a correction that connects the production and decay processes of the top quark. In fact one may incorporate the contribution of this diagram by multiplying Eq. (4.1) by a factor $[1+\xi(p,E,x_l,\cos\theta_{lt})]$, where

$$\xi(p,E,x_l,\cos\theta_{lt}) = C_F\cdot 4\pi\alpha_s\int\frac{d^3\mathbf{q}}{(2\pi)^3}\,\frac{1}{|\mathbf{q}-\mathbf{p}_t|^3}\,{\rm Re}\left[\frac{\tilde{G}^*(q,E)}{\tilde{G}^*(p,E)}\int_0^{2\pi}\frac{d\phi_{bl}}{2\pi}\,\frac{|\mathbf{q}-\mathbf{p}_t|}{\hat{\mathbf{n}}_b\cdot(\mathbf{q}-\mathbf{p}_t)+i\epsilon}\right]. \tag{4.10}$$

$\hat{\mathbf{n}}_b$ denotes the unit vector in the direction of b. After integration over $d\Omega_{\mathbf{q}}d\phi_{bl}$, one may reduce the expression to a one-parameter integral form as

$$\xi(p,E,x_l,\cos\theta_{lt}) = C_F\cdot 4\pi\alpha_s\int_0^\infty dq\left\{w_{\rm R}\,{\rm Re}\left[\frac{\tilde{G}^*(q,E)}{\tilde{G}^*(p,E)}\right] + w_{\rm I}\,{\rm Im}\left[\frac{\tilde{G}^*(q,E)}{\tilde{G}^*(p,E)}\right]\right\} \tag{4.11}$$

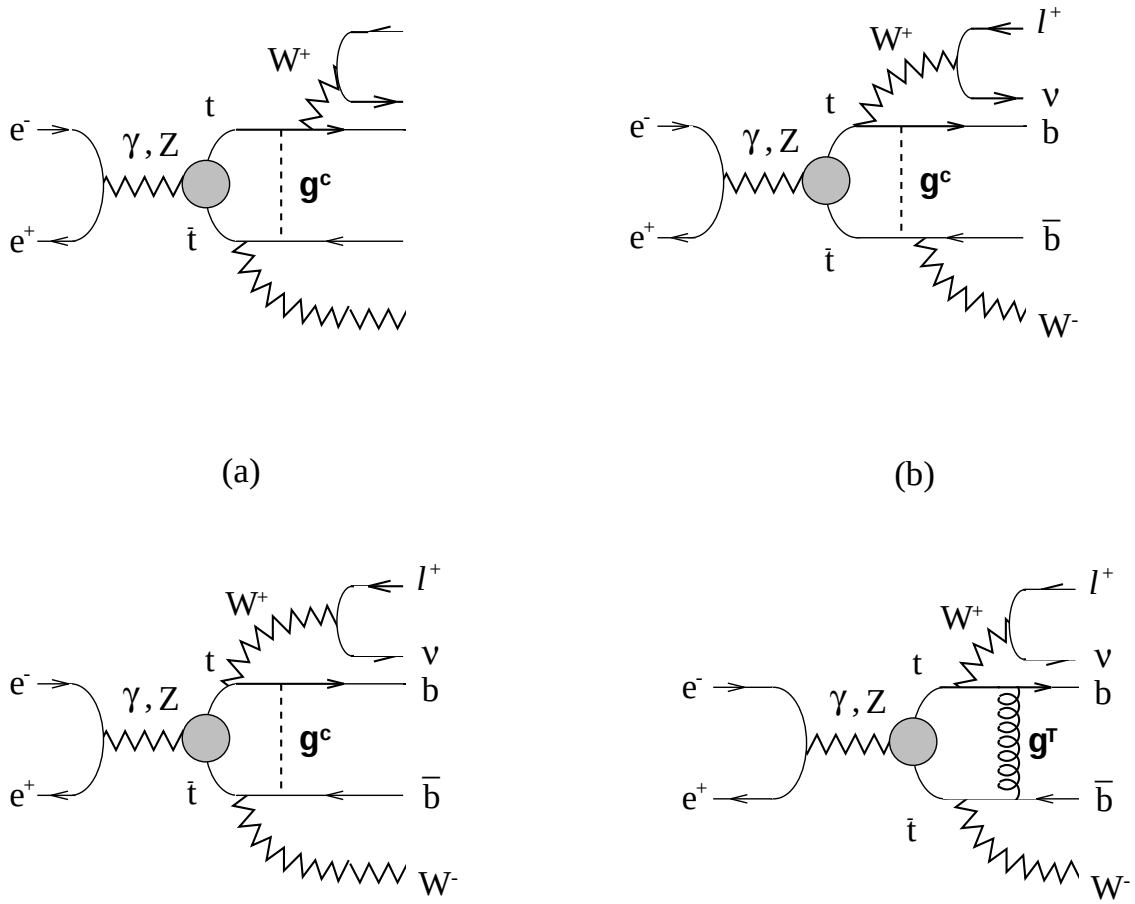

Figure 6: Diagrams for final-state interactions for $e^+e^- \to t\bar{t} \to bl^+\nu\bar{b}W^-$: (a)Coulomb-gluon exchange between t and $\bar{b}$, (b)Coulomb-gluon exchange between $\bar{t}$ and b, (c)Coulomb-gluon exchange between b and $\bar{b}$, and (d)transverse-gluon exchange between b and $\bar{b}$.

with

$$w_{\rm R} = \frac{1}{4\pi^2}\frac{q}{p^2-q^2}\left\{\theta(z_+^2-1)\cosh^{-1}|z_+| - \theta(z_-^2-1)\cosh^{-1}|z_-|\right\}, \tag{4.12}$$

$$w_{\rm I} = \frac{1}{4\pi^2}\frac{q}{|p^2-q^2|}\left\{\pi\theta\left((1+z_+)(1+z_-)\right) - \theta(1-z_+^2)\cos^{-1}(z_+) - \theta(1-z_-^2)\cos^{-1}(z_-)\right\}, \tag{4.13}$$

$$z_\pm = \frac{q/p \pm \cos\theta_{Wl}\cos\theta_{lt}}{\sin\theta_{Wl}\sin\theta_{lt}}, \quad \cos\theta_{Wl} = \frac{1+y}{1-y} - \frac{2y}{x_l(1-y)}, \quad \cos\theta_{lt} = \frac{\mathbf{p}_t\cdot\mathbf{p}_l}{|\mathbf{p}_t||\mathbf{p}_l|}. \tag{4.14}$$

Here, θ_{Wl} represents the angle between W^+ and l^+ in the t rest frame (given as a function of x_l); θ_{lt} represents the angle between t and l^+ in the $t\bar{t}$ c.m. frame ($0 \le \theta_{Wl}, \theta_{lt} \le \pi$). The inverse functions $\cosh^{-1}$ and $\cos^{-1}$ in the above formulas take their values within $[0,\infty)$ and $[0,\pi]$, respectively. $\theta(x)$ is the step function. It is understood that the principal value should be taken in the integration of the $w_{\rm R}$-term as $p \to q$.

Two noteworthy properties of $\xi(p, E, x_l, \cos\theta_{lt})$ are: (1) its l^+-angular dependence enters only through $\cos\theta_{lt}$ and is independent of the angle from the e^- beam direction or from the top-quark polarization vector, and (2) it is purely determined by the QCD interaction and free of the coupling parameters of electroweak interactions (except y).

As a non-trivial cross-check of the formula (4.11), we integrated $\xi \times \Gamma_t^{-1} d\Gamma_{t\to bl^+\nu}/dx_l d\Omega_l$ over the lepton energy-angular variables $\int dx_l d\Omega_l$ analytically and reproduced the one-parameter integral formula[10] for the final-state interaction correction (from diagram (b)) to the top-quark three-momentum distribution.

The contribution of diagram (c) (exchange of one Coulomb-gluon between b and $\bar{b}$) vanishes within our approximation. In fact one can show quite generally that the contribution of diagram (c) vanishes at $\mathcal{O}(\alpha_s)$ *provided* one calculates a cross section where the top-quark energy is integrated out; for example, the top-quark three-momentum distribution. This is not the case when one considers a cross section that depends explicitly on the top-quark energy; for example, the top-quark four-momentum distribution. Then the diagram in question *does* contribute.

It can be shown using similar techniques that the contribution of diagram (d) (exchange of one transverse-gluon between b and $\bar{b}$) gets canceled when it is added to that of the corresponding real-gluon emission diagram (interference of diagrams (e) and (f) in Fig. 7). This cancellation is consistent with the same cancellation that was found in the calculation of top-quark momentum distribution[10]. The contribution from each of these diagrams comes from the gluon momentum region $|\mathbf{k}| \lesssim \alpha_s^2 m_t$ and is in fact logarithmically divergent due to soft-gluon singularity.

Now let us compare our formulas and the argument given in the previous section. In subsections 3.b and 3.c, the $V-A$ nature of the electroweak interaction in $\bar{t}$ decay played an essential role, while this was not the case in subsections 3.a and 3.d. We find that correspondingly the $\cos\theta_{te}$ term of δ_a and $\delta\boldsymbol{\mathcal{P}}_a$ contain electroweak coupling parameters (through $C_{||}^0$) while the symmetric term of δ_a and ξ are independent of these electroweak parameters. More precisely, the $\cos\theta_{te}$ term of δ_a and $\delta\boldsymbol{\mathcal{P}}_a$ have the forms anticipated in subsections 3.b and 3.c, respectively, if the function $\psi_{\rm R}(p,E)$ is positive. Indeed, the numerical evaluation in Ref. [18] shows that $\psi_{\rm R}(p,E) \gtrsim 0$ holds in the entire threshold region. Besides, an additional

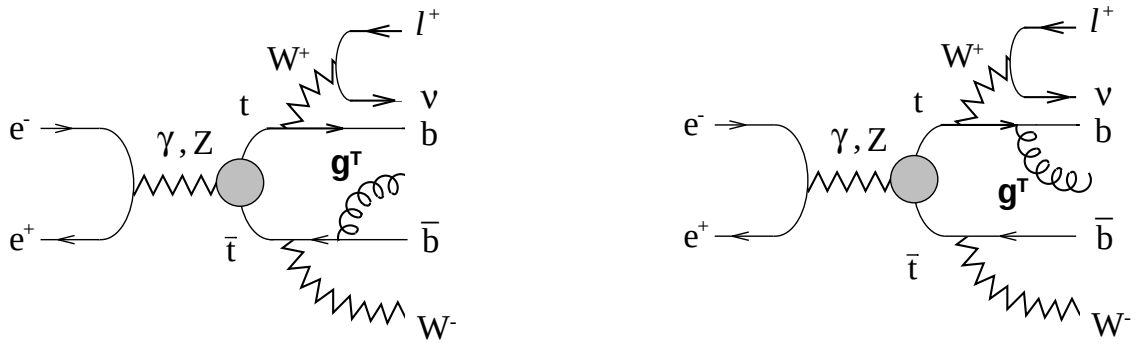

Figure 7: Diagrams for real-gluon emission process $e^+e^- \to t\bar{t} \to bl^+\nu\bar{b}W^-g$.

coefficient $\left[1-(C_{\|}^0)^2\right]$ in $\delta\boldsymbol{\mathcal{P}}_a$ can be understood within our previous argument in the extreme cases $C_{\|}^0 = \pm 1$. Namely, if the top quark is 100% polarized, there will be no contamination from the opposite spin so that the correction should disappear.

4.c Formula Including Full $\mathcal{O}(\alpha_s)$ Corrections

In summary, the energy-angular distribution of l^+ including full $\mathcal{O}(\alpha_s) = \mathcal{O}(\beta)$ corrections can be cast into a form

$$\frac{d\sigma(e^+e^- \to t\bar{t} \to bl^+\nu\bar{b}W^-)}{d^3\mathbf{p}_t dx_l d\Omega_l} = \frac{d\sigma(e^+e^- \to t\bar{t})}{d^3\mathbf{p}_t} \times \frac{1}{\Gamma_t}\frac{d\Gamma_{t\to bl^+\nu}(\boldsymbol{\mathcal{P}})}{dx_l d\Omega_l} \times (1+\xi) \tag{4.15}$$

with

$$\frac{d\sigma(e^+e^- \to t\bar{t})}{d^3\mathbf{p}_t} = \frac{d\sigma^0_{t\bar{t}}}{d^3\mathbf{p}_t} \times \left[1 + \frac{1}{2}\psi_1 + (2C_{FB}\varphi_{\rm R} + \frac{\kappa}{2}C_{\|}^0\psi_{\rm R})\cos\theta_{te}\right], \tag{4.16}$$

$$\boldsymbol{\mathcal{P}} = \boldsymbol{\mathcal{P}}_{\rm Born} + \delta\boldsymbol{\mathcal{P}}_a. \tag{4.17}$$

The above distribution is obtained as the sum of the cross sections for $e^+e^- \to t\bar{t} \to bl^+\nu\bar{b}W^-$ and $e^+e^- \to t\bar{t} \to bl^+\nu\bar{b}W^-g$. An independent emission of a gluon from the t or $\bar{t}$ side has been included in Eq. (4.1), while the interference of both has been incorporated in conjunction with the final-state interaction diagram (d) in subsection 4.b.

Experimentally the top-quark four-momentum p_t^μ will necessarily be reconstructed from the $\bar{b}W^-$ system in the study of the l^+ distribution. For the case with a gluon in the final state, we assign the "top-quark momentum" as

$$\begin{array}{lll} \text{Case (A)}: & p_t \equiv (p_{e^-}+p_{e^+}) - (p_{\bar{b}}+p_{W^-}+p_g) & \text{if} \quad (p_{\bar{b}}+p_{W^-}+p_g)^2 - m_t^2 \lesssim m_t\Gamma_t, \\ \text{Case (B)}: & p_t \equiv (p_{e^-}+p_{e^+}) - (p_{\bar{b}}+p_{W^-}) & \text{if} \quad (p_{\bar{b}}+p_{W^-})^2 - m_t^2 \lesssim m_t\Gamma_t. \end{array}$$

(See, however, the discussion in section 6.) In other kinematical configurations the cross section is suppressed. Experimentally there will be a corresponding cut in the $\bar{b}W^-$ invariant mass.

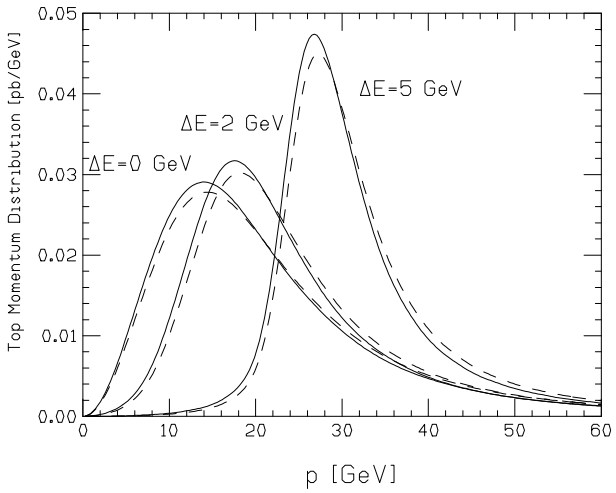

Figure 8: Top-quark momentum distributions $d\sigma/d|\mathbf{p}_t|$ obtained from Eq.(4.7) for various c.m. energies measured from the lowest lying resonance, $\Delta E = \sqrt{s} - M_{1S}$. Solid lines and dashed lines represent the distributions with and without the final-state interaction between t and $\bar{b}$ (δ_a), respectively. We set $P_{e^-} = 0$.

If both conditions in (A) and (B) are satisfied simultaneously, the gluon should necessarily be soft, and there will be no difference within our approximation between the cross sections corresponding to the above two assignments of the top-quark momentum.

5 Numerical Results

In this section we examine effects of the final-state interaction corrections to the l^+ energy-angular distribution numerically and compare the results with the qualitative argument given in section 3. We set $m_t = 175$ GeV, $\alpha_s(M_Z) = 0.118$, $P_{e^+} = 0$ and $\alpha = 1/128$ in all our analyses.

We first examine the contribution of diagram (a) in Figs. 6 (Coulomb interaction between t and $\bar{b}$) as given in Eqs.(4.7)-(4.9). Shown in Fig.8 are the top-quark momentum distribution $d\sigma/d|\mathbf{p}_t|$ for various c.m. energies measured from the lowest lying resonance,* $\Delta E = \sqrt{s} - M_{1S}$. This is calculated from the top-quark production cross section Eq.(4.7). As expected, the top-quark momentum is reduced. The effects are half in magnitude as compared to the final-state interaction corrections given in Refs.[10, 18] since only the interaction between t and $\bar{b}$ is included here.

We show angular distributions of top quarks in Figs. 9. It can be seen that the final-state interaction increases the top-quark distribution in the forward direction for $P_{e^-} = 1$. This is consistent with our argument in subsection 3.b since in leading-order approximation t and $\bar{t}$ have their spins aligned perfectly in the $\hat{\mathbf{n}}_{||}$ direction for this e^- polarization. Oppositely we see

* M_{1S} is defined as the real part of the position of the lowest lying resonance pole in the complex energy plane. The energy measured from M_{1S} is more convenient than the energy measured from the threshold ($E = \sqrt{s} - 2m_t$) when we compare different potentials in literatures.

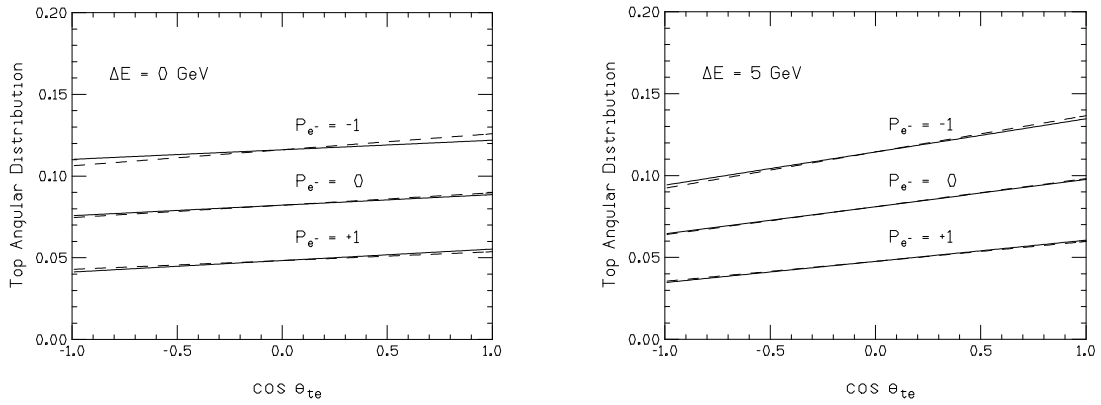

Figure 9: Top-quark angular distribution $d\sigma/d\cos\theta_{te}$ obtained from Eq.(4.7) for various electron polarizations P_{e^-}. Solid lines and dashed lines represent the distributions with and without the final-state interaction between t and $\bar{b}$ (δ_a), respectively.

that the final-state interaction decreases the top-quark distribution in the forward direction for $P_{e^-} = -1$. We note that the top quark has a natural polarization $\boldsymbol{\mathcal{P}} \simeq -0.4\hat{\mathbf{n}}_{||}$ for unpolarized e^+e^- beams. Hence, the sign of the correction is the same as in the $P_{e^-} = -1$ case. Also we show corrections to the top-quark polarization vector in Figs. 10. Although the qualitative behavior meets our expectation, the magnitude of the correction is rather small. Note that $\delta\boldsymbol{\mathcal{P}}_a$ vanishes for $P_{e^-} = \pm 1$ since $C^0_{||} = \pm 1$.

Next we investigate the irreducible (non-factorizable) correction that stems from the Coulomb interaction between $\bar{t}$ and b. The correction factor $\xi(p, E, x_l, \cos\theta_{lt})$ given in Eqs.(4.11)-(4.14) depends on four parameters. Of these, x_l and $\cos\theta_{lt}$ specify the lepton configuration. Therefore, we will examine the dependence of ξ on these two parameters for several $(p, \Delta E)$ combinations. We fix the top-quark momentum p to be the peak momentum of the distribution for each ΔE; see the top-quark momentum distributions in Fig. 8. Shown in Figs. 11 are 3-dimensional plots of ξ as a function of x_l and $\cos\theta_{lt}$. One sees that in the figures ξ takes comparatively large positive values for either 'small x_l and $\cos\theta_{lt} \simeq -1$' or 'large x_l and $\cos\theta_{lt} \simeq +1$'. On the opposite side, in the other two corners of the x_l-$\cos\theta_{lt}$ plane ξ becomes small or becomes negative for smaller ΔE. The typical magnitude of ξ is 10-20%, which would be reasonable size for an $\mathcal{O}(\alpha_s) = \mathcal{O}(\beta)$ correction. These qualitative features hold also for ξ at p off the peak of top-quark momentum distribution. These features of the correction factor ξ are consistent with our qualitative argument in section 3.

We made a cross-check of our numerical results for ξ by numerically integrating $\xi \times \Gamma_t^{-1} d\Gamma_{t\to bl^+\nu}/dx_l d\Omega_l$ over the lepton energy-angular vairables $\int dx_l d\Omega_l$ and comparing to the final-state interaction corrections to top-quark momentum distribution given in Refs.[10, 18].

6 Conclusion and Discussion

In this paper we considered the differential distribution of l^+ from the semi-leptonic decay of top quark, where the parent top quark is produced in $e^+e^- \to t\bar{t}$ near threshold. Particularly, we

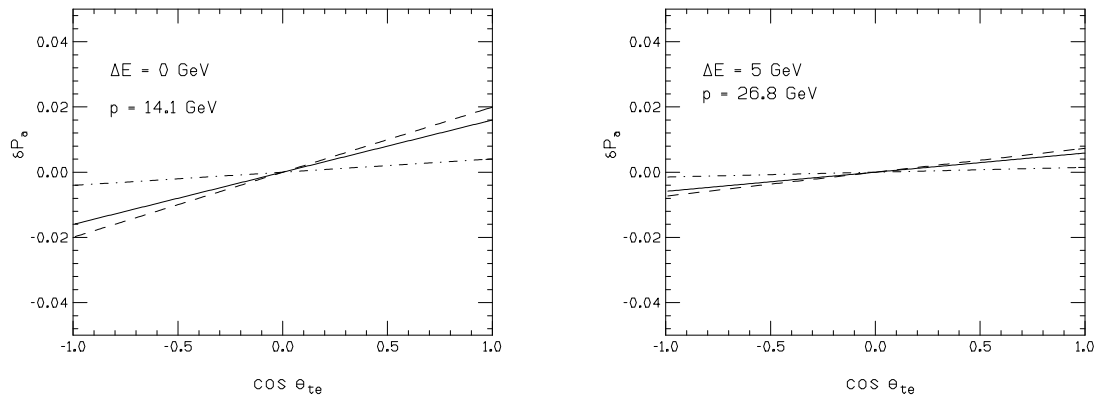

Figure 10: Final-state interaction correction to the $\hat{\mathbf{n}}_{||}$ component of the top-quark polarization vector, $\delta\boldsymbol{\mathcal{P}}_a$, for $P_{e^-} = +0.8$ (solid line), 0 (dash line), -0.8 (dotdash line).

have calculated the final-state interaction corrections (rescattering corrections) to the energy-angular distribution of lepton in the top quark decay. Also we have explicitly written down the l^+ energy-angular distribution $d\sigma(e^+e^- \to t\bar{t} \to bl^+\nu\bar{b}W^-)/d^3\mathbf{p}_t dx_l d\Omega_l$ including the full $\mathcal{O}(\alpha_s) = \mathcal{O}(\beta)$ corrections near threshold.

We presented numerical studies of the various effects of the final-state interaction corrections. All numerical results can be understood qualitatively from intuitive pictures. Attractive forces between t and $\bar{b}$ and between $\bar{t}$ and b modify not only the momentum distribution of bW^+ or $\bar{b}W^-$ system but also the top-quark polarization vector and the lepton energy-angular distribution.

- The effect of Coulomb-gluon exchange between $\bar{b}$ and t, when integrated over $\bar{b}W^-$ phase-space, can be regarded as a correction to the top-quark production process. The effect can be incorporated by modifying the top-quark production cross section and the top-quark polarization vector. The top-quark momentum distribution is shifted to take a smaller average momentum due to the attraction by $\bar{b}$. Also since $\bar{b}$ is emitted preferrably in the t spin direction, the attraction generates a $\cos\theta_{te}$ distribution of the top quark as well as modifies the top-quark polarization vector.

- The Coulomb interaction between b and $\bar{t}$ causes a non-factorizable correction with respect to the production and decay processes of the top quark. The lepton distribution is deformed in favor of the kinematical configurations "small E_l and emitted in $\bar{t}$ direction" or "large E_l and emitted in t direction", which can be understood as originating from the attraction of b in the direction of $\bar{t}$.

- Corrections from the gluon exchange between b and $\bar{b}$ turn out to vanish when the top-quark energy is integrated out.

Without the non-factorizable effect ξ, the l^+ angular distribution is dependent only on the polar angle from the polarization vector of the parent top quark in its rest frame. The final-state interaction brings in another direction into the problem, the direction of $\bar{t}$, which is a completely new feature in comparison to the decays of free polarized top quarks.

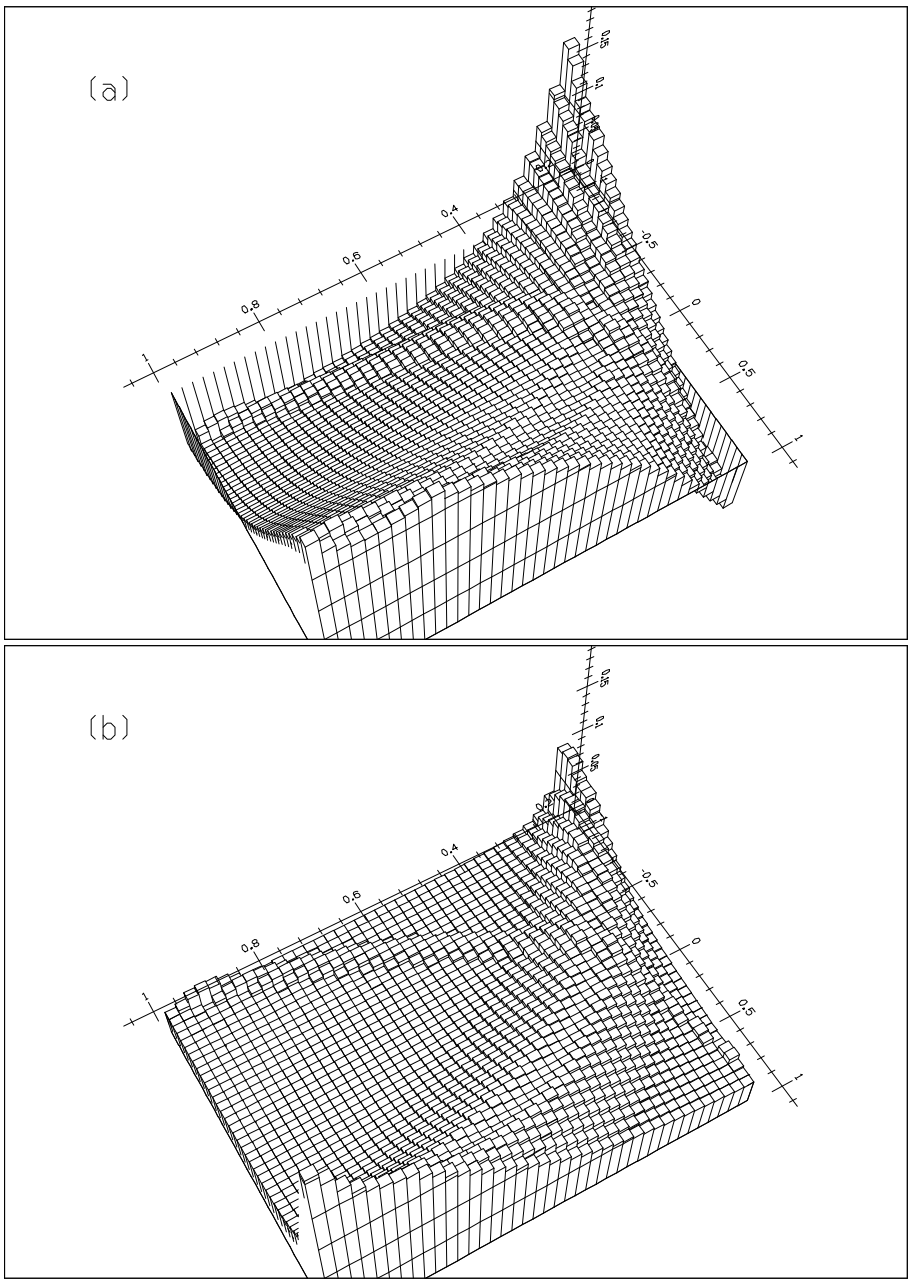

Figure 11: Three-dimensional plots of ξ as a function of x_l (x-axis) and $\cos\theta_{te}$ (y-axis) at the peak momenta of the $|\mathbf{p}_t|$-distribution in Fig. 8: (a)$\Delta E = 0$ GeV and $|\mathbf{p}_t| = 14.1$ GeV, (b)$\Delta E = 5$ GeV and $|\mathbf{p}_t| = 26.8$ GeV.

In subsection 4.c, we assumed a perfect assignment of top-quark momentum in cases (A) and (B) for defining the distribution formula, Eq.(4.15). In real experiments, however, miss-assignment of top-quark momentum will be inevitable whenever there is real gluon radiation in final state because of the typical jet-clustering algorithm that will be used. For instance, when a gluon is indistinguishable from a b-jet, the top-quark momentum reconstructed by clustering may be off-shell; rather grouping the gluon on the other side (with $\bar{b}$) would result in an on-shell momentum.[†] Ref.[10] studied how this miss-assignment alters the top-quark three-momentum distribution near threshold and found that the correction is less than a few percent; the clustering algorithm assumed in that paper, however, is somewhat unrealistic. The effect of the miss-assignment was also studied in Ref.[27] in the open-top region ($\sqrt{s} \gg 2m_t$) using a Monte Carlo generator and with more realistic experimental assumptions. It was shown that the effects on the top-quark invariant-mass distribution and on the angular distributions are substantial at $\sqrt{s} = 400$ GeV (for $m_t = 175$ GeV) and increase in magnitude and in complexity as the c.m. energy is raised. Clearly, in our case, we need more detailed studies to see how the similar effect may influence our results. For this purpose, studies based on a Monte Carlo generator that produces fully-differential distribution including full $\mathcal{O}(\alpha_s)$ corrections near threshold would be necessary.

The authors wish to thank M. Jeżabek and J.H. Kühn for enlightening discussion.

References

[1] V.S. Fadin and V.A. Khoze, *JETP Lett.* **46**, 525 (1987); *Sov. J. Nucl. Phys.* **48**, 309 (1988).

[2] M. Strassler and M. Peskin, *Phys. Rev.* **D43**, 1500 (1991).

[3] Y. Sumino, K. Fujii, K. Hagiwara, H. Murayama, and C.-K. Ng, *Phys. Rev.* **D47**, 56 (1993).

[4] H. Murayama and Y. Sumino, *Phys. Rev.* **D47**, 82 (1993).

[5] M. Jeżabek, J.H. Kühn and T. Teubner, *Z. Phys.* **C 56** (1992) 653.

[6] M. Jeżabek and T. Teubner, *Z. Phys.* **C 59** (1993) 669.

[7] P. Igo-Kemenes, M. Martinez, R. Miquel, and S. Orteu, Talk given at *the Workshop on Physics and Experiments with Linear e^+e^- Colliders* (Waikoloa, Hawaii, April 1993).

[8] J.H. Kühn, in: F.A. Harris et al. (eds.), *Physics and Experiments with Linear e^+e^- Colliders*, Singapore: World Scientific, 1993, p.72.

[9] K. Melnikov and O. Yakovlev, *Phys. Lett.* **B324**, 217 (1994).

[10] Y. Sumino, PhD thesis, University of Tokyo 1993 (unpublished).

[†] There is no ambiguity of assigning the gluon to the production of $t\bar{t}$ since real gluon radiation in the top-quark production process is suppressed near threshold.

[11] V. Fadin, V. Khoze, and A. Martin, *Phys. Rev.* **D49**, 2247 (1994); *Phys. Lett.* **B320**, 141 (1994).

[12] K. Fujii, T. Matsui and Y. Sumino, *Phys. Rev.* **D50**, 4341 (1994).

[13] W. Mödritsch and W. Kummer, Universität Wien preprint, TUW-94-06, (1994); W. Kummer and W. Mödritsch, TUW-94-14, (1994).

[14] Y. Sumino, *Acta Phys. Polonica* **B25** 1837 (1994).

[15] M. Jeżabek, in: T. Riemann and J. Blümlein (eds.), *Physics at LEP200 and Beyond*, *Nucl. Phys.* **37 B** *(Proc.Suppl.)* (1994) 197.

[16] R. Harlander, M. Jeżabek, J.H. Kühn and T. Teubner, *Phys. Lett.* **B 346** (1995) 137.

[17] W. Mödritsch, Preprint TUW-95-22, hep-ph/9509342.

[18] R. Harlander, M. Jeżabek, J. Kühn, and M. Peter, *Z. Phys.* **C73**, 477 (1997).

[19] M. Jeżabek and J. Kühn, *Phys. Lett.* **B316**, 360 (1993).

[20] M. Jeżabek, *Acta Phys. Polonica* **B 26** (1995) 789.

[21] M. Jeżabek and J.H. Kühn, *Nucl. Phys.* **B 314** (1989) 1.

[22] M. Jeżabek and J.H. Kühn, *Nucl. Phys.* **B 320** (1989) 20.

[23] A. Czarnecki, M. Jeżabek and J.H. Kühn, *Nucl. Phys.* **B 351** (1991) 70;
A. Czarnecki and M. Jeżabek, *Nucl. Phys.* **B 427** (1994) 3.

[24] M. Jeżabek and J.H. Kühn, *Phys. Rev.* **D 48** (1993) R1910; erratum *Phys. Rev.* **D 49** (1994) 4970

[25] K. Melnikov and O. Yakovlev, *Nucl. Phys.* **B471**, 90 (1996).

[26] W. Beenakker, A. Chapovsky and F. Berends, hep-ph/9706339.

[27] C. Schmidt, *Phys. Rev.* D54, 3250 (1996).